Aerosol and Air Quality Research, 15: 1844–1854, 2015

ISSN: 1680-8584 print / 2071-1409 online
doi: 10.4209/aaqr.2015.05.0380

Impact of Meteorological Parameters and Gaseous Pollutants on $PM_{2.5}$ and PM_{10} Mass Concentrations during 2010 in Xi'an, China

Ping Wang[1,3], Junji Cao[1,2*], Xuexi Tie[1], Gehui Wang[1], Guohui Li[1], Tafeng Hu[1], Yaoting Wu[3], Yunsheng Xu[3], Gongdi Xu[3], Youzhi Zhao[3], Wenci Ding[3], Huikun Liu[1], Rujin Huang[1], Changlin Zhan[4]

[1] *Key Laboratory of Aerosol Chemistry & Physics, SKLLQG, Institute of Earth Environment, Chinese Academy of Sciences, Xi'an 710075, China*
[2] *Institute of Global Environmental Change, Xi'an Jiaotong University, Xi'an 710049, China*
[3] *Qiongzhou University, Sanya 722000, China*
[4] *School of Environmental Science and Engineering, Hubei Key Laboratory of Mine Environmental Pollution Control and Remediation, Hubei Polytechnic University, Huangshi 435003, China*

ABSTRACT

Mass concentrations of $PM_{2.5}$ and PM_{10} from the six urban/rural sampling sites of Xi'an were obtained during two weeks of every month corresponding to January, April, July and October during 2010, together with the six meteorological parameters and the data of two precursors. The result showed that the average annual mass concentrations of $PM_{2.5}$ and PM_{10} were 140.9 ± 108.9 µg m^{-3} and 257.8 ± 194.7 µg m^{-3}, respectively. Basin terrain constrains the diffusion of $PM_{2.5}$ and PM_{10} concentration spatially. High concentrations in wintertime and low concentrations in summertime are due to seasonal variations of meteorological parameters and cyclic changes of precursors (SO_2 and NO_2). Stepwise Multiple Linear Regression (MLR) analysis indicates that relative humidity is the main factor influencing on meteorological parameter. Entry MLR analysis suggests that SO_2 from local coal-burning power plants is still the primary pollutant. Trajectory cluster results of $PM_{2.5}$ at BRR indicate that the entrained urban pollutants carried by the westerly or winter monsoon forms the dominant regional pollution sources in winter and spring. Ultraviolet (UV) aerosol index verified the source and pathway of dust storm in spring.

Keywords: Xi'an; $PM_{2.5}$ and PM_{10}; Meteorological parameters; Gaseous pollutants.

INTRODUCTION

Atmospheric particulate $PM_{2.5}$ (particles with aerodynamic equivalent diameter ≤ 2.5 µm), also known as the lungs of particulate matter, is considered as an important indicator of air quality because of its effects on human health (Haywood and Boucher, 2000; IPCC, 2007, Tie *et al.*, 2009). The extent of $PM_{2.5}$ concentration depends on both direct emissions and the quantity of gaseous precursors, such as SO_2 and NO_2, etc. as well as meteorological conditions.

The major source of SO_2 is exclusively from coal-burning power plants and the NO_2 in Xi'an is exclusively from vehicles. In the last decade, SO_2 was the primary gaseous pollutant in China, but recent studies from ground measurement (Zhang *et al.*, 2012; Cao *et al.*, 2013), satellite observation (Chan and Yao, 2008; Geng *et al.*, 2009), and model simulation (He *et al.*, 2007) show that NO_x (including NO_2) is the No. 1 gaseous pollutant after the desulfurization of coal-fired power plant plumes, the elimination of coal-fired boilers in manufacturing facilities and small power plants, and the conversion of domestic coal utilization to cleaner fuels, etc. (van der A *et al.*, 2006). These results suggest that China's long-term efforts to restrict SO_2 emissions were successful during the 11th Five-Year-Plan (FYP) (2005–2010); in the same time, the emission control target in the 12th FYP (2011–2015) is continuation of SO_2 emission control at 8% of reduction and NO_x reduction at 10% for the first time (http://www.zhb.gov.cn/).

Meteorological factors are also important in controlling $PM_{2.5}$ pollutions in a relatively short time scale. Several studies investigated the effects of climate alteration on $PM_{2.5}$ with different methods, including inputting meteorological parameters on climate models and chemical transport models, and using in-site measurements of meteorological date and archived data (Fang *et al.*, 2009; Tai *et al.*, 2010; Xu *et al.*, 2011). Conventional meteorological parameters such as

* Corresponding author.
Tel.: 86-29-8832-6488; Fax: 86-29-8832-0456
E-mail address: cao@loess.llqg.ac.cn

wind direction (WD), wind speed (WS), temperature (T), relative humidity (RH), surface pressure (PS) and planetary boundary layer height (PBLH) etc. are expected to have important effects on $PM_{2.5}$ variation to some extent. For example, WS can alter the dispersion state of the atmosphere, while WD provides information on the path of pollutants (Luvsan *et al.*, 2012; Tie *et al.*, 2015). Low PBLH, a strong temperature inversion, and descending air motion under weak surface WS can increase the frequency of haze phenomenon in China (Jones *et al.*, 2010; Hu *et al.*, 2012), particularly in some cities located in basin regions during winter, such as Beijing and Xi'an (Chen *et al.*, 2012; Lin *et al.*, 2012). However, there is no clear linear relationship between meteorological parameters (i.e., wind speed, temperature or relative humidity) and the concentration of $PM_{2.5}$ due to effects of chemical reactions and transformations (Chan and Yao, 2008). For example, sulfate concentration is expected to increase with temperature rising due to the faster SO_2 oxidation, but on the other hand, semi-volatile components, such as nitrate and organics, are expected to decrease because the transformation from the particle phase into the gas phase is easily formed at low temperature. An increase of cloud can cause an increase of sulfate and nitrate due to the enhancement in sulfate heterogeneous reactions in water (Zhang *et al.*, 2013). However, an increase in precipitation causes a decrease in $PM_{2.5}$ concentrations through scavenging, so it is necessary to have a comprehensive understanding of the uncertain sensitivity between meteorological parameters and $PM_{2.5}$ and PM_{10} concentrations.

Xi'an (34°16′N, 108°54′E), the capital city of Shaanxi province, is located in the Guanzhong Plain (Fig. 1). Xi'an has a temperate, semi-arid climate with northeast prevailing wind. An annual precipitation is 550 millimeters and an annual average of temperature is 13.7°C. Dust storm often occurs during March and April. Geographically, Xi’an is a basin surrounded by Qinling Mountainin in south and the Loess Plateau in north and west. Moreover, only one outlet in the northeast of Xi’an determines that the pollutants in Xi’an cannot be easily dispersed out. Furthermore, regional source is easily transported from adjacent district throughout the outlet. For example, coal-dominant energy consumption in northeast part of Shaanxi province produces large amount pollutants, which can be transported through the outlet to the Guanzhong Plain (Zhao *et al.*, 2015). Previous findings show that the average $PM_{2.5}$ concentration in Xi’an reached its the highest level during winter (375.2 μg m^{-3}) and summer (130.8 μg m^{-3}) during 2003 (Cao *et al.*, 2012a). The air quality in Xi’an has been degrading for years and especially in winter, and the poor air quality posts adverse effects on local residents (Cao *et al.*, 2007; Huang *et al.*, 2012).

The objective of this study is to discuss the variation of $PM_{2.5}$ and PM_{10} mass concentrations in Xi'an driven by the meteorological parameters and the emissions of their precursors. The discussion includes: (1) $PM_{2.5}$ and PM_{10}

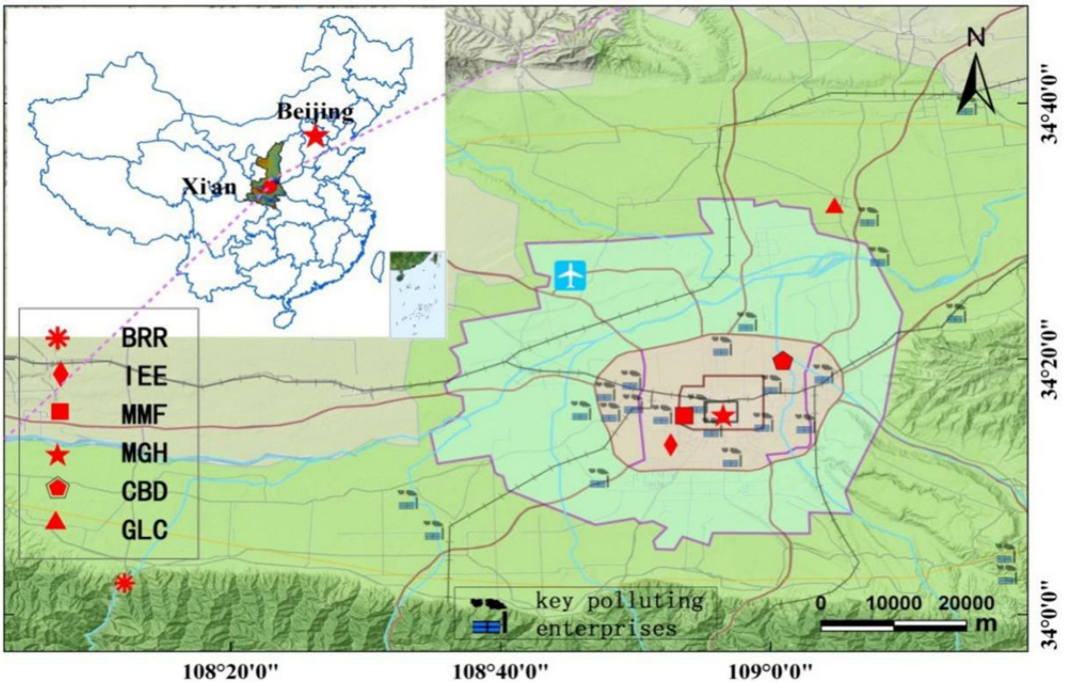

Fig. 1. (a) location of Xi’an in China, and (b) the location of six sampling sites (four urban sites and two suburban sites), nineteenth automatic monitor stations, twenty-four key polluting enterprises (labeling classification of industrial nature), and the traffic network with old city wall and ring roads during 2010 in Xi’an, China. Four urban sampling sites respectively are: Chan-ba ecological district (CBD) (34°20′18.54″N, 109°01′21.66″E), Municipal government hall (MGH) (34°16′01.08″N, 108°56′58.49″E), Micro motor factory (MMF) (34°15′59.65″N, 108°53′55.22″E), Institute of earth environment, Chinese academy of science (IEE) (34°13′49.77″N, 108°52′58.72″E); Two rural sampling sites: upwind district of Gaoling county (GLC) (34°32′05.34″N, 109°05′12.11″E), downwind area of Black river reservoir (BRR) (34°02′51.05″N, 108°12′21.27″E).

characteristics, (2) the key meteorological factors, which affect PM mass concentration and the conversion of gaseous SO_2 and NO_2 to $PM_{2.5}$ and PM_{10}, (3) effects of potentially regional sources on $PM_{2.5}$. This study will provide necessary reference information for the local government to develop atmospheric environment pollution control strategies and an emergency plan.

MATERIAL AND METHODOLOGY

The Monitoring Locations

The six urban/rural sampling sites are shown in Fig. 1, illustrating their topography, key polluting enterprises and traffic route. Four urban sites include Institute of earth environment, Chinese academy of science (IEE) in the south, Micro motor factory (MMF) in the west, Municipal government hall (MGH) in the Downtown zone, and Chan-ba ecological district (CBE) in the east. Two rural sites include Gaoling county (GLC) in the northeast and a reference station of Black river reservoir (BRR) in the southwest. The reason for choosing BRR station as a reference to investigate potentially regional sources is that it is located on the edge of Qingling Mountains.

$PM_{2.5}$ and PM_{10} Sampling Analysis

Daily $PM_{2.5}$ and PM_{10} samples were collected during 4 periods, including 1) 12 to 25 January; 2) 14 to 27 April; 3) 12 to 25 July; and 4) 12 to 25 October, 2010, corresponding to winter, summer, spring and fall, respectively. Minivals (Airmetrics Corp., Springfield, OR, USA) were installed at each station, with 10 m above ground level. These samplers used the Whatman quartz microfiber filters (QM/A), with 47 mm in diameter and operated at 5 L min^{-1} of inlets. Filter blanks were collected from each site during the sampling time. Prior to sampling, all the samplers were carefully checked and calibrated. A total 56 pairs of $PM_{2.5}$ and PM_{10} filters were collected at the six sampling sites.

$PM_{2.5}$ and PM_{10} mass concentrations of the sample filters were analyzed by using an electronic microbalance, with 1 µg sensitivity (MC5; Sartorius, Goettingen, Germany) in a controlled environment (35–45% RH at 20–23°C).

Data of Gaseous Pollutants and Meteorological Parameters

Daily average SO_2 and NO_2 concentrations (Fig. 2(d)) at eleven automatic monitor stations were obtained from the website of Xi'an environment monitoring center (http://www.xianemc.gov.cn).

Meteorological information was obtained from GDAS (Global Data Assimilation System) of NOAA with 24-hour resolution (ftp://arlftp.arlhq.noaa.gov/pub/archives/gdas1/), including wind direct, wind speed, temperature, relative humidity, surface pressure and PBLH (Figs. 2(a)–2(c)).

Trajectory Clusters and Remote Sensing Retrieval

Backward trajectory analysis was calculated by using the HYSLPIT4.8 (Hybrid Single Paricle Lagrangian Integrated Trajectory) model from NOAA Air Resources Laboratory (http://www.arl.noaa.gov/ready/hysplit4.8 html), with the 6-hourly archive meteorological data from the GDAS (1° × 1°). Three-day backward trajectories at the end point of BRR reference site in Xi'an with a height of 500 m above

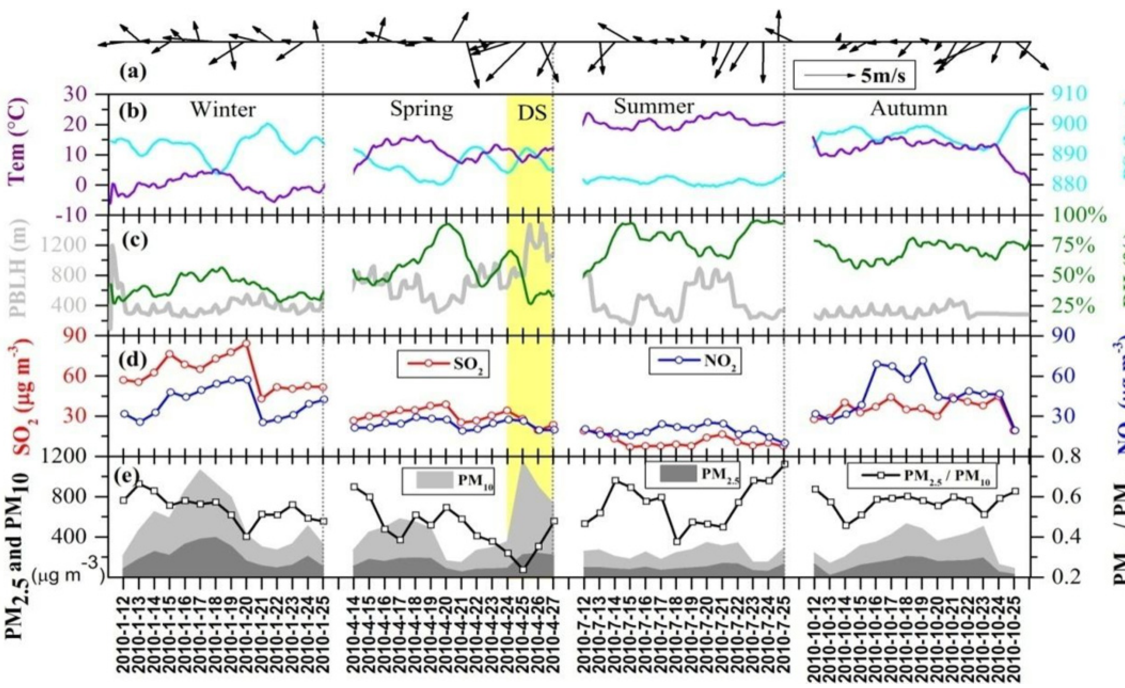

Fig. 2. Time-series of 24-hour meteorological parameters with (a) wind directions and wind speed (m s^{-1}), (b) temperature (°C) and surface press (hPa), (c) planetary boundary layer height (m) and relative humidity (%) during the study period (12–25 Jan., 14–27 Apr., 12–25 Jul. and 12–25 Oct.) in 2010 over Xi'an. Time-series of 24-hour average concentrations of (d) SO_2 and NO_2, (e) $PM_{2.5}$ and PM_{10} with ratio of $PM_{2.5}/PM_{10}$ during the same study period as above.

the ground level are calculated at 10:00 LST (Local Standard Time) per day during the observation period. The individual trajectories were grouped into 2–3 clusters (Fig. 5 and Table 3) by using the clustering tool in TrajStat a GIS Trajectory Analysis Tool (MeteoInfo) (http://www.ready.noaa.gov/HYSPLIT.php).

Giovanni is a web-based application developed by the NASA Goddard Earth Sciences Data and Information Services Center (GES DISC). It provides a simple and easy way to explore, visualize, analyze, and access a vast amount of Earth science remote sensing and model data (http://disc.sci.gsfc.nasa.gov/giovanni/overview/index.html). Ozone Monitoring Instrument (OMI) Ultraviolet (UV) Aerosol Index (AI) of Aura satellite is most sensitive to absorbing aerosols above the planetary boundary layer, i.e., smoke plumes and dust (de Graaf *et al.*, 2005) (Fig. 6).

RESULTS AND DISCUSSION

$PM_{2.5}$ and PM_{10} Spatial and Seasonal Variations

Fig. 2 shows six daily average meteorological parameters and, SO_2, NO_2, $PM_{2.5}$, PM_{10} mass concentrations, the ratio of $PM_{2.5}/PM_{10}$ during the 4 periods. Table 1 summary the seasonal average concentrations (mean concentration ± standard deviation) of the meteorological parameters, SO_2, NO_2, $PM_{2.5}$ and PM_{10} during observed date in 2010. The average concentration of $PM_{2.5}$ is 140.9 ± 108.9 µg m^{-3} with an arrange from 23.1 to 562.6 µg m^{-3}. This is about 13 times higher than that of the World Health Organization (WHO) standard (10 µg m^{-3}), 8 times higher than U.S. standard (15 µg m^{-3}), 5 times higher than EU $PM_{2.5}$ (25 µg m^{-3}), and 3 times higher than that of the latest average annual standard (GB 3095-2012) issued by the Chinese Ministry of Environmental Protection (35 µg m^{-3}) (http://www.envir.gov.cn/law/airql.htm). PM_{10} is 257.8 ± 194.7 µg m^{-3} (range value: 46.1–926.8 µg m^{-3}), and is twice of the average annual standard of China (100 µg m^{-3}). The PM general variation is similar to that in previous studies in Xi'an (Han *et al.*, 2008; Shen *et al.*, 2008, 2009, 2011).

Fig. 3 presents the daily variations of $PM_{2.5}$ and PM_{10} mass concentrations at six sampling sites spatially. The peaks of PM_{10} in six sites found during a dust storm time (Fig. 3(b) with yellow maker) indicates that the course particles loading in PM_{10} is caused by a constant trend and a low $PM_{2.5}/PM_{10}$

Table 1. Seasonal average concentrations (mean concentration ± standard deviation) of five meteorological parameters, SO_2, NO_2, $PM_{2.5}$ and PM_{10} from GDAS of NOAA, eleven automatic monitor stations and six sampling sites, respectively, during observed date in 2010.

		Wintertime (12/01–25/01) 14	Springtime (14/04–27/04) 14	Summertime (12/07–25/07) 14	Autumntime (12/10–25/10) 14	Av. ± std[g] 56
Meteorological parameters	WS[a] (m s^{-1})	2.49 ± 0.47	2.80 ± 0.88	2.13 ± 0.65	2.19 ± 0.78	2.40 ± 0.74
	T[b] (°C)	–0.26 ± 2.90	10.89 ± 3.58	20.90 ± 2.04	11.86 ± 3.13	10.85 ± 8.11
	RH[c] (%)	39.70 ± 8.24	56.34 ± 17.23	79.47 ± 13.94	69.99 ± 6.90	61.38 ± 19.28
	PS[d] (hpa)	892.9 ± 3.71	886.67 ± 4.00	881.26 ± 1.43	897.02 ± 3.40	889.46 ± 6.85
	PBLH[e] (m)	386.1 ± 106.93	747.99 ± 259.09	452.14 ± 248.61	310.16 ± 51.49	474.1 ± 248.67
Precursors	SO_2 (µg m^{-3})	62.01 ± 12.37	29.92 ± 5.51	11.19 ± 4.31	35.49 ± 7.36	34.65 ± 19.93
	NO_2 (µg m^{-3})	40.45 ± 11.57	23.89 ± 3.54	18.98 ± 4.28	45.91 ± 16.03	32.31 ± 15.06
$PM_{2.5}$ (µg m^{-3})	BRR	122.94 ± 26.84	106.44 ± 148.36	39.14 ± 20.29	53.94 ± 37.97	80.61 ± 84.00
PM_{10} (µg m^{-3})		253.84 ± 102.95	328.77 ± 407.27	106.87 ± 45.24	133.03 ± 94.44	211.22 ± 234.31
	GLC	149.78 ± 100.72	103.97 ± 75.42	46.29 ± 13.34	108.71 ± 54.28	103.20 ± 76.88
		326.97 ± 180.48	306.87 ± 251.50	159.51 ± 60.18	223.31 ± 98.05	254.94 ± 173.26
	IEE	258.43 ± 176.44	111.55 ± 72.32	132.84 ± 89.22	148.49 ± 68.78	162.83 ± 121.95
		371.86 ± 171.3	330.83 ± 170.86	141.69 ± 53.05	220.72 ± 102.59	266.27 ± 159.27
	MMF	243.89 ± 149.67	177.53 ± 90.75	113.41 ± 50.78	154.07 ± 69.72	172.23 ± 106.2
		441.58 ± 254.33	340.94 ± 220.86	231.64 ± 107.96	152.31 ± 99.04	291.42 ± 208.71
	MGH	231.95 ± 162.7	122.00 ± 100.88	126.33 ± 31.68	163.45 ± 90.52	160.26 ± 112.51
		399.32 ± 232.19	375.95 ± 265.58	160.77 ± 48.80	255.35 ± 111.41	300.34 ± 206.67
	CBE	193.64 ± 131.88	206.88 ± 102.12	83.86 ± 53.27	166.02 ± 79.74	160.21 ± 102.46
		203.45 ± 134.29	354.29 ± 231.7	109.68 ± 78.32	209.29 ± 89.93	215.03 ± 166.43
	Sum[f]	202.59 ± 138.53	145.84 ± 104.73	91.52 ± 60.95	126.48 ± 89.05	140.92 ± 108.89
		336.33 ± 198.35	339.65 ± 261.59	153.18 ± 80.04	200.56 ± 104.86	257.83 ± 194.68
$PM_{2.5}/PM_{10}$ (%)		60.24	42.94	59.75	63.06	54.66

[a] WS = Wind speed.
[b] T = 2 meter temperature.
[c] RH = 2 meter relative humidity.
[d] PS = Surface pressure.
[e] PBLH = Planetary boundary layer height.
[f] Sum = Average concentration ± standard deviation of six sapling sites.
[g] Av. ± std. = Seasonal average concentration ± standard deviation.

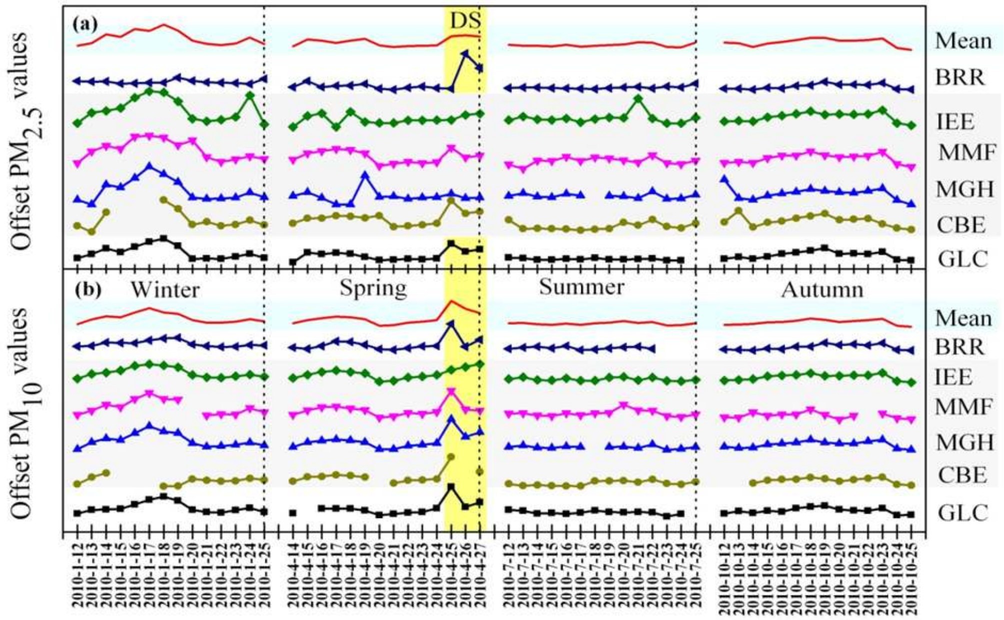

Fig. 3. The diurnal variations of average concentrations of $PM_{2.5}$ and PM_{10} from observed data of six sampling sites during 2010 in Xi'an.

ratio at six sites. While, a "sawtooth" variation of fine particles $PM_{2.5}$ indicates that local sources could be the major contributors, especially in wintertime (Fig. 3(a)). A "pear-shaped" geography of Xi'an surrounded by three mountains with an outlet to northeast determines that the pollutants cannot disperse easily (Fig. 1), which could support this argument above (Zhu *et al.*, 2010; Wang *et al.*, 2015).

Seasonal variations are shown in Fig. 2(e) and Table 1, which indicate that $PM_{2.5}/PM_{10}$ mass concentrations are high in wintertime and low in summertime. This is attributed to the seasonal variations of meteorological parameters and cyclic changes of precursors from source emission. The highest concentrations of $PM_{2.5}$ and PM_{10} can be found in wintertime (except for during a dust storm time) for following reasons. Firstly, the strong temperature inversion (average concentration ± standard deviation: –0.3 ± 2.9°C) and descending in air motions in PBLH (386.1 ± 106.9 m) allows pollutants to accumulate in a shallow layer (Table 1). However, on the other hand, the low surface wind speed (2.5 ± 0.5 m s^{-1}) is not favor to diffuse SO_2 and NO_2 concentrations (62.1 ± 12.4 µg m^{-3} and 40.5 ± 11.6 µg m^{-3}, respectively) (Table 1). In addition, in winter heating period, $PM_{2.5}$ and PM_{10} concentrations at the three sampling sites (MMF, MGH and IEE) in urban area are obviously higher than that of two sites in suburban area (GLC and BRR) (Table 1). This suggests that central heating has a serious impact on $PM_{2.5}$ and PM_{10} in central urban area. This conclusion is also verified in precious studies via the PMF analysis, which show that coal combustion contribution of percentage of 21% for PM_1 during 2008 (the contribution of coal combustion is 21% for PM_1) (Shen *et al.*, 2010), 52.2% (the sum of coal combustion and secondary aerosols) for $PM_{2.5}$ during 2009 (Cao *et al.*, 2012b) and 18.5% for $PM_{2.5}$ during 2010 (Wang *et al.*, 2015) in Xi'an. According to Fig. 4(a), the spatial distributions of SO_2 from coal-burning energy consumption can also verify that the precursors of $PM_{2.5}$ are mainly concentrated around the central urban area. The variation of the peak points of $PM_{2.5}$ concentration in wintertime is influenced by the interaction of driving forces of meteorological factor (low temperature, low wind speed and low PBLH) and high emissions of SO_2.

In springtime, compared to $PM_{2.5}$ (except at reference site BRR), the peaks of PM_{10} mass concentrations in the six sampling sites are almost equal (Figs. 3(a) and 3(b)), which indicates that a dust storm time (25, 26, 27/04, 2010) influences on PM_{10} with northwest prevailing wind at mean speed of 4.4 m s^{-1} (Fig. 2(a)). During a dust storm time, the lowest $PM_{2.5}/PM_{10}$ ratio (0.3) is observed in 25/04, which is also the lowest ratio over the whole observed time, then followed by 0.4 in 26/04 and 0.5 in 27/04 (Fig. 2(e)). Those facts indicate that the coarse mode particles are the dominant PM type during the dust storm.

The lowest concentrations of $PM_{2.5}$ and PM_{10} over the entire observed time appeared in summertime and whose trend remains stable (Figs. 2(e) and 3). This is caused by the accelerated homogeneous and heterogeneous reactions between SO_2 and radicals, such as OH, H_2O_2, etc., with a high average temperature (20.9 ± 2.0°C) (Table 1). But the high temperature is also expected to decrease $PM_{2.5}$ species compositions, for instance, semi-volatile components: nitrate and organics, because their dynamic equilibrium of the transformation changes from the particle phase into the gas phase (Cao *et al.*, 2007). For example, ammonium nitrate volatilizes partially at a temperature over 20°C, meanwhile it forms gaseous nitric acid. When the temperature rises over 25°C, the volatilization completes (Calvo *et al.*, 2013). Moreover, based on the statistical analysis from 1970 to 2009 in Xi'an weather station (34.3°N, 109.0°E, 399 m above sea level), the average annual precipitation mainly occurs in July and September (http://www.tianqi.com/xian/index.html).

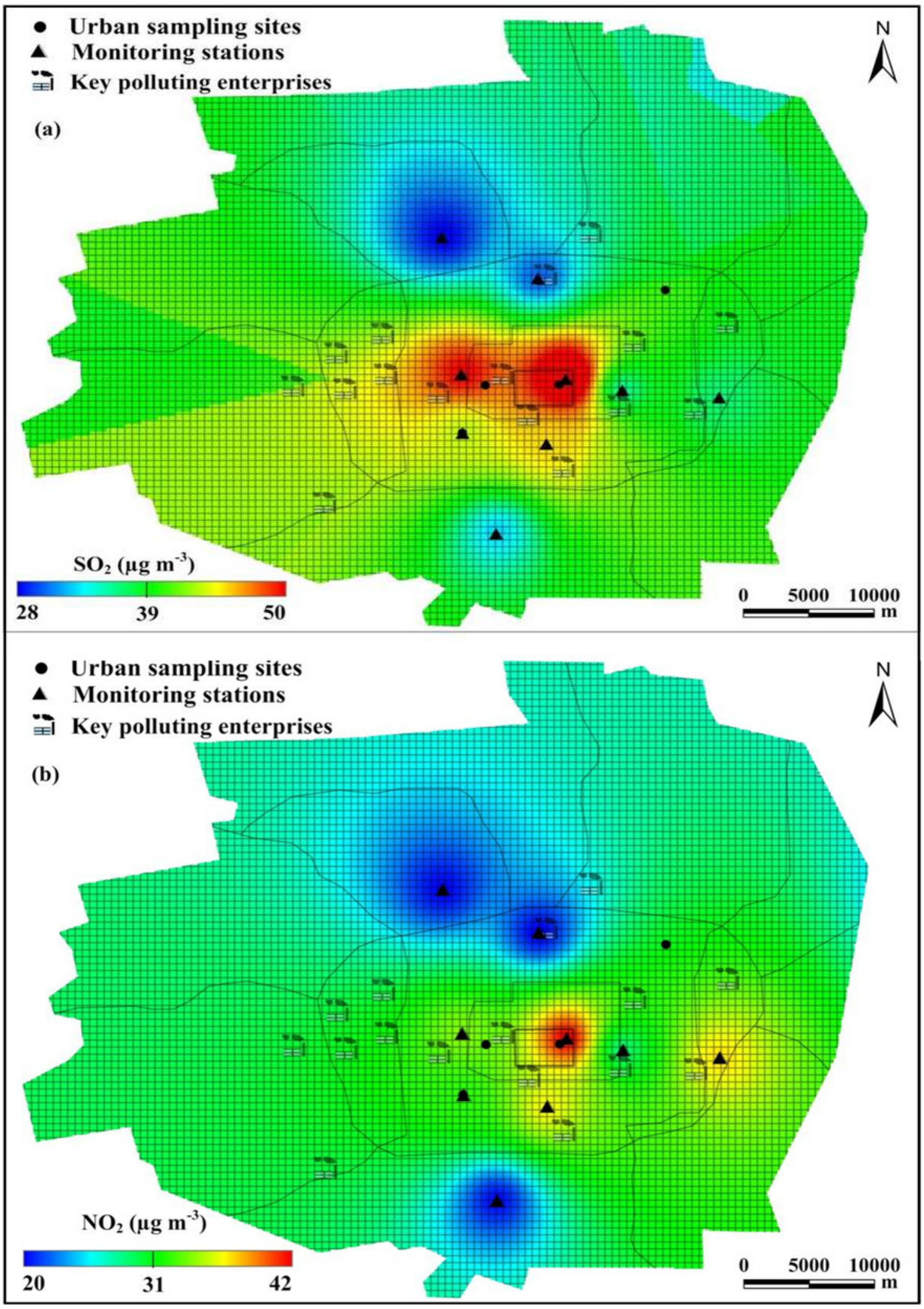

Fig. 4. Spatial distribution of annual average SO_2 (a) and NO_2 (b) via inverse distance interpolation of ArcGIS at urban area during 2010 in the main city area of Xi'an (grid with 50 × 50 m).

Therefore, the low concentrations of $PM_{2.5}$ and PM_{10} can be explained by that the combining result of the rainout effect and suppression effect of RH exceeds the accelerating effect of RH. Thus, the low $PM_{2.5}/PM_{10}$ values in summertime may be caused by the rainout and the decrease of the semi-volatile components in PM at a high temperature.

The moderate concentrations of $PM_{2.5}$ and PM_{10} (Fig. 3(e)) in autumn could be explained by the low average PBLH (310.2 ± 51.5 m) and the air stagnant caused by a low wind speed (2.2 ± 0.8 m s^{-1}) (Table 1).

In short, basin terrain constrains $PM_{2.5}/PM_{10}$ spatial diffusion. Seasonal variations of meteorological parameters and cyclic changes of precursors from source emission are the main causes for the $PM_{2.5}/PM_{10}$ seasonal distribution.

Factors Mainly Influencing to $PM_{2.5}$ and PM_{10} Concentrations, Respectively

Meteorological parameters have complex effects on the total PM concentration due to no clear linear relationship between each other (Chan and Yao, 2008). However, based on the knowledge of PM and five meteorological factors mentioned above, the stepwise MLR can be applied to extract the major influencing factors (Stehr *et al.*, 2000). All Variance Inflation Factors (VIF) of independent variables are less than 10, indicating that it does not have significant collinearity effects before model diagnosis (Tong *et al.*, 2005). Table 2 presents stepwise MLR results, together with parameter estimation (T-test) of independence variable and model formula estimation (F-test and R). The result shows that the main contributors to mass concentration of $PM_{2.5}$ are the precursor of SO_2, temperature and RH. In contrast, the main contributors to mass concentration of PM_{10} are NO_2, wind speed, surface pressure and RH. RH, as a co-existent influencing factor for mass concentrations of $PM_{2.5}$ and PM_{10} can indicate the major liquid-phase/heterogeneous reaction in the process of PM formation. However, there is an interesting result showed by MLR analysis between RH and concentrations of $PM_{2.5}$ and PM_{10}. The result indicates a negative correlation coefficient between RH and PM, which is not common in other cases. Thus, more in-depth study should be conducted. In addition, sulfate formation through SO_2 oxidation dominates mass concentrations of $PM_{2.5,}$ and nitrate formation through NO_2 oxidation is the dominant substance in PM_{10}. Those findings are consistent with previous study (Yao *et al.*, 2002).

Recent studies show that SO_2 emissions started decreasing in China after 2006 (Lu *et al.*, 2010). Nitrogen oxides would be the major pollutant to be concerned about in the present and future. Satellite observation and model simulation also detected and predicted a strong increase of NO_2 in Eastern China (Li *et al.*, 2010a). In particular, Shanghai had a significantly linear increase of NO_2 column concentrations with about 20% increase rate annually during the period of 1996–2005 (He *et al.*, 2007). However, SO_2 from local coal-burning power plants is the major primary pollutants, and the majority of it is produced by its raw material-based economic development and west-east electricity transmission project in Xi'an.

Contribution Rates of SO_2 and NO_2 to $PM_{2.5}$ and PM_{10}

It is a common understanding that point sources (mainly coal-burning) emit high level of SO_2, and relatively low level of NO_2. However, mobile sources (mainly fossil fuel-burning) emit high level of NO_2. Based on the observed data from eleven automatic states of Xi'an environment monitoring center, the relative contributions from point sources (stationary) and mobile sources to $PM_{2.5}$ and PM_{10} are investigated through entry MLR is applied (Tong *et al.*, 2005; van der A *et al.*, 2006). The mathematical expression of the model is

$$[PM_{2.5}] = \alpha_1\,[SO_2] + \beta_1\,[NO_2] + \delta_1, \tag{1}$$

$$[PM_{10}] = \alpha_2\,[SO_2] + \beta_2\,[NO_2] + \delta_2, \tag{2}$$

where α_1, α_2, β_1 and β_2 are the linear coefficients between $[PM_{2.5}]$, $[PM_{10}]$ and $[SO_2]$ and $[NO_2]$, respectively, and δ_1, δ_2 are the intercept, respectively. Before the parameterizations of α_1 and β_1, and α_2 and β_2, are calculated, the collinearity effects of SO_2 and NO_2 on the estimates of regression coefficient are diagnosed. The VIF is 1.55 (< 4) suggesting that the collinearity is not significant. Results show that standardized parameters of α_1, β_1, α_2 and β_2 are 0.486, 0.175, 0.395 and 0.007 respectively, which suggest that the emission from coal-burning makes a major contribution to $PM_{2.5}$ and PM_{10}, with up to 48.6% and 39.5%, respectively The contribution of vehicle emission are 17.5% and 0.7%, and the contribution of other sources are 33.9% and 59.8%. The contribution from SO_2 to $PM_{2.5}$ and PM_{10} outweighing that from NO_2 proves that the dominant polluting gas is SO_2 in Xi'an again. Previous study shows that about 73% of SO_2 emitted from power plant contributes 11% of the total PM_{10} and 12% of the total $PM_{2.5}$. 31% of NO_2 from

Table 2. Stepwise multiple linear regression among $PM_{2.5}$, PM_{10}, SO_2, NO_2 and six meteorological parameters, respectively, during the observed period in 2010.

Parameter	WS[a]	T[b]	RH[c]	PS[d]	PBLH[e]	SO_2	NO_2	Constant	R[f]	F-test	Sig.[g]
	X_1	X_2	X_3	X_4	X_5	X_6	X_7	X_0			
Slope (β)		5.826	–1.138			3.561		27.977			
Coe. (γ)[i]		–0.293	–0.41			0.602					
T-test		3.358	–1.965			5.555		0.577			
Sig.		0.001	0.055			0		0.566			
Model	$[PM_{2.5}] = 3.561 \times [SO_2] + 5.826 \times [T] - 1.138 \times [RH] + 27.977$								0.691	15.869	0
Slope (β)	61.502		–4.189	–7.293			3.798	6731.88			
Coe. (γ)[h]	0.407		–0.501	0.035			0.269				
T-test	2.451		–4.075	–2.224			2.698	2.3			
Sig.	0.018		0	0.031			0.009	0.026			
Model	$[PM_{10}] = 3.798 \times [NO_2] - 61.502 \times [WS] - 4.189 \times [RH] + 7.293 \times [PS] + 6731.88$								0.656	9.61	0

[a] WS = Wind Speed.
[b] T = 2 meter temperature.
[c] RH = 2 meter relative humidity.
[d] PS = Surface pressure.
[e] PBLH = Planetary boundary layer height.
[f] R = Correlation coefficient.
[g] Sig. = Significance.
[h] Coe. (γ) = Partial correlation coefficient.
Observed period = 12/01–25/01, 14/04–27/04, 12/07–25/07, and 12/10–25/10 in 2010.

traffic sectors (fossil fuel burning) is accountable for 7% of the total PM_{10} and 10% of the total $PM_{2.5}$ in the year of 2003 in Huabei region, China (Stehr *et al.*, 2000). The contributions of SO_2 and NO_2 to $PM_{2.5}$ and PM_{10} in 2010 in Xi'an are quite different from those in 2003 in Huabei region. The major uncertainties depend on the two independent variables of regression model and co-emission of SO_2 and NO_2 by power plant and transformation sources.

Effects of Potentially Regional Source on $PM_{2.5}$

The contributions of local source to $PM_{2.5}/PM_{10}$ via emitting precursors of SO_2 and of NO_2 have been mentioned above. The effects of regional source on $PM_{2.5}$ studied by trajectory clusters are elaborated as follow. Trajectory analyses provide an insight into the impact of long-range air transport on PM variation at receptor site (Li *et al.*, 2010b; He *et al.*, 2012). Taking $PM_{2.5}$ of BRR at reference sampling site as an example, Fig. 5 shows the mean trajectory of the 2–3 clusters and their percentages to the total number of trajectories. $PM_{2.5}$ concentrations are associated with the trajectories and grouped according to selected pollution trajectory criteria of seasonal average values for $PM_{2.5}$ in BRR (Table 2). Then each group of data is summarized for statistical analysis (Table 3). It is generally that the long distance air mass responds to regional source and the short air mass responds to local source. Uncertainty of trajectory clusters could be caused by the selected threshold of the polluting trajectory from different seasons. This determines that which air mass travelling at receptor site is considered as a polluting trajectory. It can be seen from Table 3 that polluting trajectory numbers of winter, spring, summer and autumn corresponding to seasonally observed data (1 × 14 day) are 6, 3, 7 and 4, respectively. The mean value of polluting trajectory numbers selected in descending order is spring (333.7 ± 203.4 µg m^{-3}) > winter (146.7 ± 24.2 µg m^{-3}) > autumn (99.0 ± 20 µg m^{-3}) > summer (52.5 ± 21.1 µg m^{-3}). As it shows in Fig. 5, the long distance air masses are dominant in winter (including cluster 1 of 83.3%) and spring (66.7%), and the short distance air mass is the major type in summer (71.4%) and autumn (75%). The entrained urban pollutants carried by the westerly or winter monsoon forms the dominant regional pollution sources in winter and spring (e.g., Lanzhou of Gansu and Yinchuan of Ningxia). However, in spring (Fig. 5(b)), high levels of external polluting trajectory (333.7 µg m^{-3}) may be a reasonable explanation due to the dilution of dust particulates in the dust storm time, which is consistent with results of impact of Gobi desert dust on aerosol chemistry of Xi'an (Cao *et al.*, 2005; Wang *et al.*, 2009).

The results of UV aerosol index analysis turn out to be consistent with trajectory analysis of air mass in Fig. 5. The data and results showed in Fig. 6, which also illustrates the

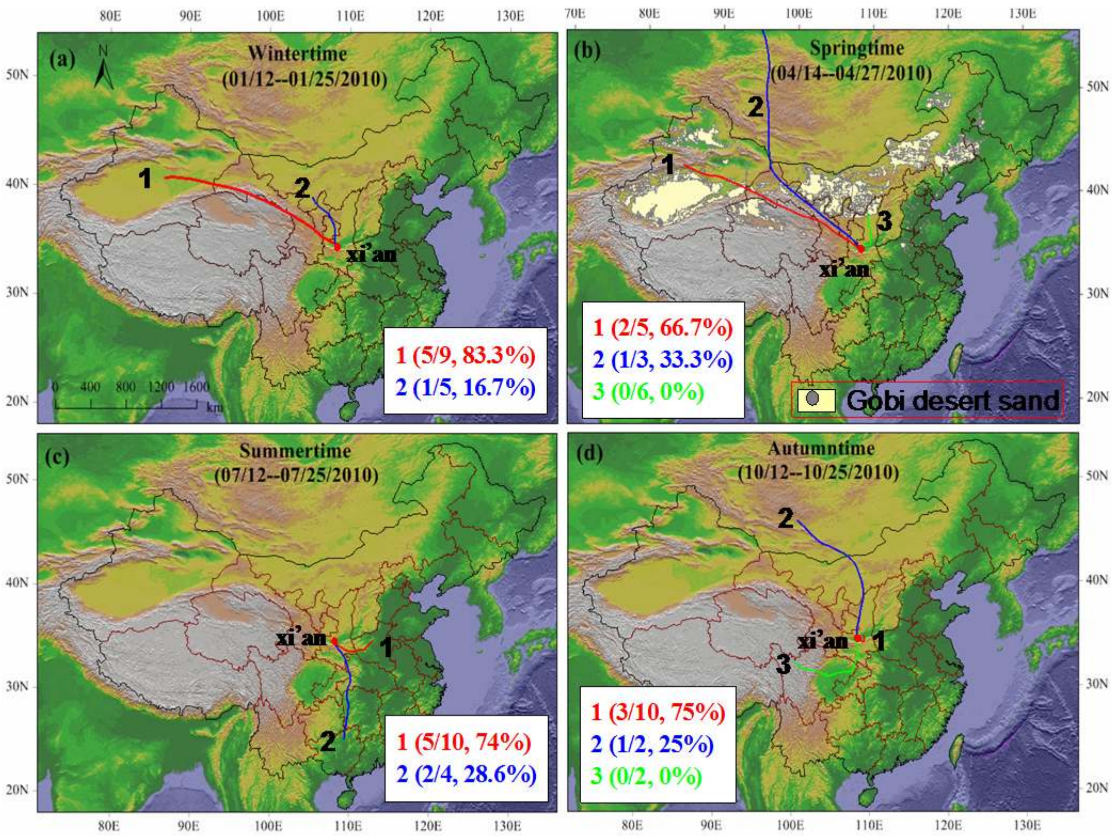

Fig. 5. Clusters of 72-hours air mass backward trajectories arriving at 500 m above ground level at10:00 LST for (a) 12 to 25 January, (b) 14 to 27 April, (c) 12 to 25 July and (d) 12 to 25 October during 2010 at BRR reference sampling site in Xi'an during 2010. 1 (5/9, 83.3%) mean number of trajectory cluster (number of polluting trajectory/number of trajectory, percentage of polluting trajectory in cluster to total polluting trajectory).

Table 3. Cluster statistics result of 72-hours air mass backward trajectories arriving at 500m above ground level at18:00 LST (Local Standard Time) at BRR reference sampling site in Xi'an for (a) 12 to 25 January, (b) 14 to 27 April, (c) 12 to 25 July and (d) 12 to 25 October over 2010.

period	Cluster	Cluster Trajectories			Pollution Cluster Trajectories		
		Number	Ratio (%)	Av. ± std[a]. (μg m^{-3})	Number	Ratio (%)	Av. ± std. (μg m^{-3})
Wintertime (12/01–25/01)	1	9	64.3	121.5 ± 24.8	5	83.3	139.2 ± 17.7
	2	5	35.7	294.76 ± 94.1	1	16.7	184.2 ± 0
	All	14	100.0	122.9 ± 26.8	6	100.0	146.7 ± 24.2
Springtime (14/04–27/04)	1	5	35.7	121.9 ± 119.7	2	66.7	229.8 ± 134.5
	2	3	21.4	205.6 ± 291.3	1	33.3	541.3 ± 0
	3	6	42.9	44.0 ± 31.8	0	0.0	0 ± 0
	All	14	100.0	106.4 ± 148.4	3	100.0	333.7 ± 203.4
Summertime (12/07–25/07)	1	10	71.4	39.4 ± 23.2	5	71.4	54.3 ± 25
	2	4	28.6	38.5 ± 12.9	2	28.6	48.1 ± 10.9
	All	14	100.0	39.1 ± 20.3	7	100.0	52.5 ± 21.1
Autumntime (12/10–25/10)	1	10	71.4	56.2 ± 39.9	3	75.0	104.2 ± 21
	2	2	14.3	80.4 ± 4.7	1	25.0	83.7 ± 0
	3	2	14.3	16.4 ± 11.3	0	0.0	0 ± 0
	All	14	100.0	53.9 ± 38	4	100.0	99.0 ± 20

[a] Av. ± std. = Average concentration ± standard deviation.
Cluster method: the Euclidean distance.
Select pollution trajectory criteria: respectively seasonal average $PM_{2.5}$ concentration in BRR reference sampling site.

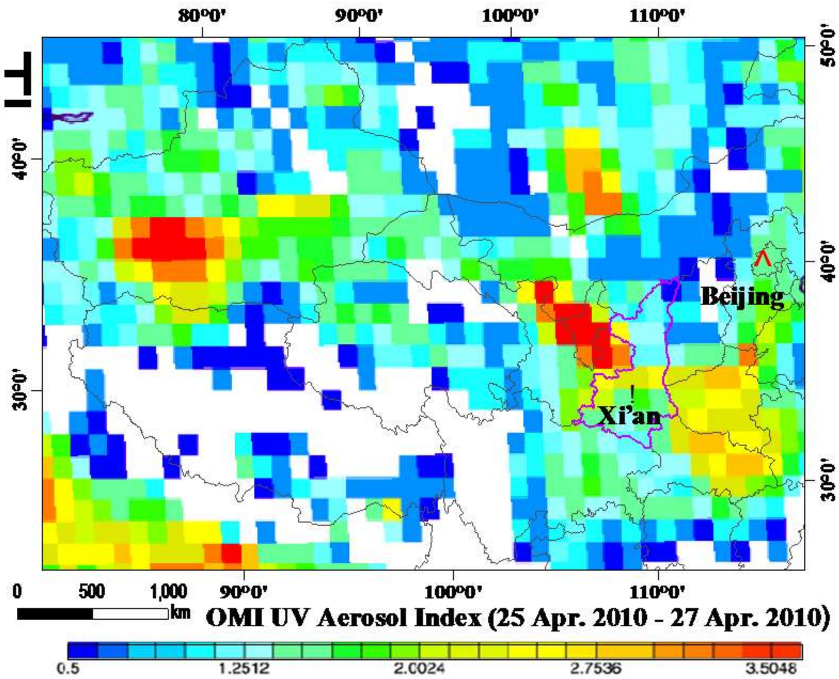

Fig. 6. UV aerosol index of a dust storm (25 Apr. 2010–27 Apr. 2010) inversing satellite imagery of OMI O_3 with spatial resolution (1° × 1°) in Xi'an.

source (Taklimakan Desert in Xinjiang and Gobi Desert in Inner Mongolia) and pathway (Hexi corridor) during a dust storm time. In short, effect of seasonally regional source on $PM_{2.5}$ in BRR reference site based on percentage of polluting trajectory to total trajectory is possible.

CONCLUSION

The average concentrations of $PM_{2.5}$ and PM_{10} in 2010 are 140.9 ± 108.9 μg m^{-3}, 257.8 ± 194.7 μg m^{-3}, respectively. Wind speed in calm and basin terrain constrains PM spatial diffusion. Seasonal variations of meteorological parameters and cyclic changes of precursors from source emission are the main causes of $PM_{2.5}/PM_{10}$ seasonal distribution.

Factors that influence on $PM_{2.5}$ from stepwise MLR analysis application are SO_2, temperature and RH. While NO_2, wind speed, surface pressure and RH are the major ones for PM_{10}. RH as the co-existing factor is the main meteorological parameter, indicating the major liquid-phase/heterogeneous reaction in the process of PM formation.

Entry MLR analysis demonstrates that coal-burning (mostly SO_2) and vehicle emission (mostly NO_2) contribute 48.6% and 33.9%, and 17.5% and 0.7% of the total $PM_{2.5}$ and PM_{10}, respectively. This indicates that SO_2 from local coal-burning power plants is still the primarily polluting gas in Xi'an.

Trajectory cluster results of $PM_{2.5}$ at BRR indicate that the dominant regional sources in winter and spring could be contributed by the Westerly or winter monsoon invasion entrained urban pollutants. And the UV aerosol index verifies the source and pathway of a dust storm in spring.

ACKNOWLEDGEMENTS

This work was supported by the "Strategic Priority Research Program" of the Chinese Academy of Sciences (XDB05060500), the National Natural Science Foundation of China (NSFC 41275186, 41430424), Hainan Marine Science and Technology Promotion (SQ2014KJXH0010), Foundation of Hainan Educational Committee (Hjkj2012_44). We thank the Xi'an City Environmental Monitoring Station Sampling for the help and support, and Giovanni online tools of the NASA Goddard Earth Sciences Data and Information Services Center (GES DISC).

REFERENCES

Calvo, A.I., Alves, C., Castro, A., Pont, V., Vicente, A.M. and Fraile, R. (2013). Research on Aerosol Sources and Chemical Composition: Past, Current and Emerging Issues. *Atmos. Res.* 120: 1–28.

Cao, J., Wang, Q., Chow, J.C., Watson, J.G., Tie, X., Shen, Z., Wang, P. and An, Z. (2012a). Impacts of Aerosol Compositions on Visibility Impairment in Xi'an, China. *Atmos. Environ.* 59: 559–566.

Cao, J., Xu, H., Xu, Q., Chen, B. and Kan, H. (2012b). Fine Particulate Matter Constituents and Cardiopulmonary Mortality in a Heavily Polluted Chinese City. *Environ. Health Perspect.* 120: 373–378.

Cao, J., Chow, J.C., Lee, F.S. and Watson, J.G. (2013). Evolution of $PM_{2.5}$ Measurements and Standards in the US and Future Perspectives for China. *Aerosol Air Qual. Res.* 13: 1197–1211.

Cao, J.J., Lee, S.C., Zhang, X.Y., Chow, J.C., An, Z.S., Ho, K.F., Watson, J.G., Fung, K., Wang, Y.Q. and Shen, Z.X. (2005). Characterization of Airborne Carbonate over a Site near Asian Dust Source Regions during Spring 2002 and Its Climatic and Environmental Significance. *J. Geophys. Res.* 110: D03203.

Cao, J.J., Lee, S.C., Chow, J.C., Watson, J.G., Ho, K.F., Zhang, R.J., Jin, Z.D., Shen, Z.X., Chen, G.C., Kang, Y.M., Zou, S.C., Zhang, L.Z., Qi, S.H., Dai, M.H., Cheng, Y. and Hu, K. (2007). Spatial and Seasonal Distributions of Carbonaceous Aerosols over China. *J. Geophys. Res.* 112: 1–9.

Chan, C.K. and Yao, X. (2008). Air Pollution in Mega Cities in China. *Atmos. Environ.* 42: 1–42.

Chen, J., Zhao, C.S., Ma, N., Liu, P.F., Göbel, T., Hallbauer, E., Deng, Z.Z., Ran, L., Xu, W.Y., Liang, Z., Liu, H.J., Yan, P., Zhou, X.J. and Wiedensohler, A. (2012). A Parameterization of Low Visibilities for Hazy Days in the North China Plain. *Atmos. Chem. Phys.* 12: 4935–4950.

de Graaf, M., Stammes, P., Torres, O. and Koelemeijer, R.B.A. (2005). Absorbing Aerosol Index: Sensitivity Analysis, Application to GOME and Comparison with TOMS. *J. Geophys. Res.* 110: D01201.

Fang, M., Chan, C.K. and Yao, X. (2009). Managing Air Quality in a Rapidly Developing Nation: China. *Atmos. Environ.* 43: 79–86.

Geng, F., Zhang, Q., Tie, X., Huang, M., Ma, X., Deng, Z., Yu, Q., Quan, J. and Zhao, C. (2009). Aircraft Measurements of O_3, NO_x, CO, VOCs, and SO_2 in the Yangtze River Delta region. *Atmos. Environ.* 43: 584–593.

Han, Y., Cao, J., Posmentier, E.S., Fung, K., Tian, H. and An, Z. (2008). Particulate-associated Potentially Harmful Elements in Urban Road Dusts in Xi'an, China. *Appl. Geochem.* 23: 835–845.

Haywood, J. and Boucher, O. (2000). Estimates of the Direct and Indirect Radiative Forcing Due to Tropospheric Aerosols: A Review. *Rev. Geophys.* 38: 513–543.

He, K., Zhao, Q., Ma, Y., Duan, F., Yang, F., Shi, Z. and Chen, G. (2012). Spatial and Seasonal Variability of $PM_{2.5}$ Acidity at Two Chinese Megacities: Insights into the Formation of Secondary Inorganic Aerosols. *Atmos. Chem. Phys.* 12: 1377–1395.

He, Y., Uno, I., Wang, Z., Ohara, T., Sugimoto, N., Shimizu, A., Richter, A. and Burrows, J.P. (2007). Variations of the Increasing Trend of Tropospheric NO_2 over Central East China during the Past Decade. *Atmos. Environ.* 41: 4865–4876.

Hu, T.F., Cao, J.J., Shen, Z.X., Wang, G.H., Lee, S.C. and Ho, K.F. (2012). Size Differentiation of Individual Atmospheric Aerosol during winter in Xi'an, China. *Aerosol Air Qual. Res.* 12: 951–960.

Huang, W., Cao, J., Tao, Y., Dai, L., Lu, S.E., Hou, B., Wang, Z. and Zhu, T. (2012). Seasonal Variation of Chemical Species Associated With Short-Term Mortality Effects of $PM_{2.5}$ in Xi'an, a Central City in China. *Am. J. Epidemiol.* 175: 556–566.

IPCC (2007). Climate Change 2007: The Physical Science Basis (Contribution of Working Group I to the Fourth Assessment Report of the Intergovernmental Panel on Climate Change), Solomon, S., Qin, D., Manning, M., Chen, Z., Marquis, M., Averyt, K.B., Tignor, M. and Miller, H.L. (Eds.), Cambridge Univ. Press, New York, pp. 131–217.

Jones, A.M., Harrison, R.M. and Baker, J. (2010). The Wind Speed Dependence of the Concentrations of Airborne Particulate Matter and NO_x. *Atmos. Environ.* 44: 1682–1690.

Li, C., Zhang, Q., Krotkov, N.A., Streets, D.G., He, K., Tsay, S.C. and Gleason, J.F. (2010a). Recent Large Reduction in Sulfur Dioxide Emissions from Chinese Power Plants Observed by the Ozone Monitoring Instrument. *Geophys.*

Res. Lett. 37: L08807.
Li, H.Y., Han, Z.W., Cheng, T.T., Du, H.H., Kong, L.D., Chen, J.M., Zhang, R.J. and Wang, W.J. (2010b). Agricultural Fire Impacts on the Air Quality of Shanghai during Summer Harvest time. *Aerosol Air Qual. Res.* 10: 95–101.
Lin, M., Tao, J., Chan, C.Y., Cao, J.J., Zhang, Z.S., Zhu, L.H. and Zhang, R.J. (2012). Characterization of Regression Relationship between Recent Air Quality and Visibility Changes in Megacities at Four Haze Regions of China. *Aerosol Air Qual. Res.* 12: 1049–1061.
Lu, Z., Streets, D.G., Zhang, Q., Wang, S., Carmichael, G.R., Cheng, Y.F., Wei, C., Chin, M., Diehl, T. and Tan, Q. (2010). Sulfur Dioxide Emissions in China and Sulfur Trends in East Asia Since 2000. *Atmos. Chem. Phys.* 10: 6311–6331.
Luvsan, M., Shie, R., Purevdorj, T., Badarch, L., Baldorj, B. and Chan, C. (2012). The Influence of Emission Sources and Meteorological Conditions on SO_2 Pollution in Mongolia. *Atmos. Environ.* 61: 542–549.
Shen, Z., Cao, J., Arimoto, R., Han, Z., Zhang, R., Han, Y., Liu, S., Okuda, T., Nakao, S. and Tanaka, S. (2009). Ionic Composition of TSP and $PM_{2.5}$ during Dust Storms and Air Pollution Episodes at Xi'an, China. *Atmos. Environ.* 43: 2911–2918.
Shen Z., Cao J., Arimoto R., Han Y., Zhu C., Tian J. and Liu S. (2010). Chemical Characteristics of Fine Particles (PM_1) from Xi'an, China. *Aerosol Sci. Technol.* 44: 461–472.
Shen, Z.X., Arimoto, R., Cao, J.J., Zhang, R.J., Li, X., Du, N., Okuda, T., Nakao, S., and Tanaka, S. (2008). Seasonal Variations and Evidence for the Effectiveness of Pollution Controls on Water-Soluble Inorganic Species in Total Suspended Particulates and Fine Particulate Matter from Xi'an, China. *J. Air Waste Manage. Assoc.* 58: 1560–1570.
Shen, Z.X., Wang, X., Zhang, R., Ho, K., Cao, J. and Zhang, M. (2011). Chemical Composition of Water-soluble Ions and Carbonate Estimation in Spring Aerosol at a Semi-arid Site of Tongyu, China. *Aerosol Air Qual. Res.* 10: 360–368.
Stehr, J.W., Dickerson, R.R., Hallock-Waters, K.A., Doddridge, B.G. and Kirk, D. (2000). Observations of NO_y, CO, and SO_2 and the Origin of Reactive Nitrogen in the Eastern United States. *J. Geophys. Res.* 105: 3553–3563.
Tai, A.P.K., Mickley, L.J. and Jacob, D.J. (2010). Correlations between Fine Particulate Matter ($PM_{2.5}$) and Meteorological Variables in the United States: Implications for the Sensitivity of $PM_{2.5}$ to Climate Change. *Atmos. Environ.* 44: 3976–3984.
Tie, X., Wu, D. and Brasseur, G. (2009). Lung Cancer Mortality and Exposure to Atmospheric Aerosol Particles in Guangzhou, China. *Atmos. Environ.* 43: 2375–2377.
Tie, X.X., Zhang, Q., He, H., Cao, J.J., Han, S.Q., Gao, Y., Li, X. and Jia, X.C. (2015). A Budget Analysis of the Formation of Haze in Beijing, *Atmos. Environ.* 100: 25–36.
Tong, D.Q., Kang, D., Aneja, V.P. and Ray, J.D. (2005). Reactive Nitrogen Oxides in the Southeast United States National Parks: Source Identification, Origin, and Process Budget. *Atmos. Environ.* 39: 315–327.
van der A, R.J., Peters, D.H.M.U., Eskes, H., Boersma, K.F., Van Roozendael, M., De Smedt, I. and Kelder, H.M. (2006). Detection of the Trend and Seasonal Variation in Tropospheric NO_2 over China. *J. Geophys. Res.* 111: D12317.
Wang, P., Cao, J., Shen, Z., Han, Y., Lee, S., Huang, Y., Zhu, C., Wang, Q., Xu, H. andHuang, R. (2015). Spatial and Seasonal Variations of $PM_{2.5}$ Mass and Species during 2010 in Xi'an, China. *Sci. Total Environ.* 508: 477–487.
Wang, Y.Q., Zhang, X.Y. and Draxler, R.R. (2009). TrajStat: GIS-based Software that Uses Various Trajectory Statistical Analysis Methods to Identify Potential Sources from Long-term Air Pollution Measurement Data. *Environ. Modell. Software* 24: 938–939.
Xu, W.Y., Zhao, C.S., Ran, L., Deng, Z.Z., Liu, P.F., Ma, N., Lin, W.L., Xu, X.B., Yan, P., He, X., Yu, J., Liang, W.D. and Chen, L.L. (2011). Characteristics of Pollutants and Their Correlation to Meteorological Conditions at a Suburban Site in the North China Plain. *Atmos. Chem. Phys.* 11: 4353–4369.
Yao, X., Fang, M. and Chan, C.K. (2002). Size Distributions and Formation of Dicarboxylic Acids in Atmospheric Particles. *Atmos. Environ.* 36: 2099–2107.
Zhang, Q., Tie, X., Lin, W.L., Cao, J.J., Quan, J.N., Ran, L. and Xu, W.Y. (2013). Measured Variability of SO_2 in an Intensive Fog Event in the NCP Region, China; Evidence of High Solubility of SO_2. *Particuology* 11: 41–47.
Zhang, R.J., Tao, J., Ho, K.F., Shen, Z.X., Wang, G.H., Cao, J.J., Liu, S.X., Zhang, L.M. and Lee, S.C. (2012). Characterization of Atmospheric Organic and Elemental Carbon of $PM_{2.5}$ in a Typical Semi-Arid Area of Northeastern China. *Aerosol Air Qual. Res.* 12: 792–802.
Zhao, S., Tie, X., Cao, J., Li, N., Li, G., Zhang, Q., Zhu, C., Long, X., Li, J., Feng, T. and Su, X. (2015). Seasonal Variation and Four-year Trend of Black Carbon in the Mid-west China: The Analysis of the Ambient Measurement and WRF-Chem Modeling. *Atmos. Environ., in Press,* doi: 10.1016/j.atmosenv.2015.05.008.
Zhu, C.S., Cao, J.J., Tsai, C.J., Shen, Z.X., Ho, K.F. and Liu, S.X. (2010). The Indoor and Outdoor Carbonaceous Pollution during Winter and Summer in Rural Areas of Shaanxi, China. *Aerosol Air Qual. Res.* 10: 550–558.

Received for review, May 31, 2015
Revised, August 4, 2015
Accepted, August 14, 2015